



## Inference on seismic fragility and risk estimates of concrete bridges in Quebec

Pedro A. C. Bandini<sup>1\*</sup>, Patrick Paultre<sup>2</sup>

<sup>1</sup>Postdoctoral fellow, Department of Civil and Building Engineering, Université de Sherbrooke, Sherbrooke, Canada

<sup>2</sup>Professor, Department of Civil and Building Engineering, Université de Sherbrooke, Sherbrooke, Canada

\*[pedro.bandini@usherbrooke.ca](mailto:pedro.bandini@usherbrooke.ca) (Corresponding Author)

### ABSTRACT

System seismic fragility analyses based on Gaussian mixture seismic demand models have been deemed less biased compared to other multivariate probabilistic seismic demand model (MPSDM) approaches due to its inherent flexibility for density modeling. Nonetheless, no further verification had been provided to validate the accuracy of the Gaussian mixture-based approach, which is addressed in this paper. Fragility analysis are a versatile probabilistic tool for seismic performance assessment typically employed in post-event planning and retrofitting prioritization of transportation networks. Analytical fragility functions of multicomponent structures are commonly built upon MPSDMs, which in turn rely on simplifying hypotheses on the distribution of component seismic demands and their interactions. To avoid the introduction of modeling error, a nonparametric bootstrapping technique is used to construct system fragility functions for a case-study bridge located in Eastern Canada. From the bootstrap fragility replications, the corresponding mean annual frequencies of damage state exceedance are estimated to give an indication of bias for three different MPSDM strategies. Typical strong assumptions such as lognormality and linear dependence are here investigated. Accordingly, significant error may be propagated from the demand model into risk estimates depending on the importance of the component's fragility to the whole system vulnerability, and the GM model shows satisfactory performance.

Keywords: fragility analysis, bridges, seismic risk, seismic demand, bootstrap.

### INTRODUCTION

Intermediate steps of an analytical seismic fragility analysis may include the construction of a model that establishes a probabilistic relationship between the structural response and the earthquake intensity measure (IM): the probabilistic seismic demand model (PSDM) [1]. In the case of multicomponent structures, such as highway bridges, the seismic performance can be assessed at the component and system levels, each one with distinct usage and importance. Often, component level damages are used to estimate repair actions and costs, while system-level performance are obtained from the combination of component damages and often relates to outcomes such as lane closures, and load or speed restrictions [2]. Past studies proposed methodologies to develop PSDMs that consider the contribution of multiple critical components based on system reliability and acknowledging the existence of correlation between pairs of structural component responses [3]. One example is the framework proposed by [4] for creation of multivariate probabilistic seismic demand models (MPSDM), which has been broadly employed in analytical fragility analyses of highway bridges since then (e.g., [5,6]).

Fragility functions are inherently uncertain quantities subject to multiple sources of both aleatory and epistemic uncertainty. One of these sources is related to the hypotheses adopted in the development of probabilistic seismic demand models [7]. Due to its simplicity and tractability, component seismic demand is often assumed to be lognormally distributed. Lognormality of engineering demand parameters (EDP) (i.e., the seismic demand) is a heritage of the typical assumption on intensity measures (e.g., peak ground acceleration or spectral quantities) and has been validated in studies that used either single-degree-of-freedom or two-dimensional frame models (e.g., [8]). Conversely, it has been rejected as a general assumption in the case of bridges, while the importance of the error carried into fragility analysis depends on how far the model is from reality (e.g., [9,10]). With respect to the dependence between pairs of component responses, more complex nonlinear relationships within bridge components have been observed [11]. Accordingly, some approaches have been proposed to avoid this assumption and model a nonlinear dependence (e.g., [10,12]). The assumption of linear dependence, however, is commonly made for the sake

of simplicity. This hypothesis may introduce significant bias into fragility estimates depending on how good the fitted model represents the observed seismic response.

In a recent study performed by the authors [10] on a specific bridge in Eastern Canada, the fragility analyses based on Gaussian mixture seismic demand models were deemed less biased than other MPSDM approaches due to its inherent flexibility. At that point, however, no further verification was provided to check the accuracy of the proposed approach. The analyses presented here are thus aimed to address this limitation. To this end, bootstrap-based fragility curves are generated, allowing the statical inference on the fragility functions for the same case-study bridge. Finally, from the bootstrap fragility curve replications, the corresponding mean annual frequency of damage state exceedance are estimated to give an indication of bias of the investigated MPSDM strategies.

## GAUSSIAN MIXTURE SEISMIC DEMAND MODELS

A Gaussian mixture (GM) seismic demand model [10] is built upon GM models fit on the peak structural responses generated according to multiple-stripe analysis (MSA) [13]. In a GM model, the data points at a given stripe  $IM = im_j$  are assumed to follow a finite mixture of Gaussian distributions with unknown parameters. This probabilistic model is defined as the sum of  $n_k$  multivariate normal probability density functions (PDFs), each weighted by a probability  $\pi_k$ , with  $k = 1, \dots, n_k$ . Taking  $\mathbf{X}$  as a multivariate random variable of an observed dataset  $\mathbf{x}$  (in this case, the logarithm of the response of bridge components at a given seismic intensity level  $\mathbf{EDP}|IM = im_j$ ), the joint posterior PDF for a Gaussian mixture is thus defined by:

$$f(\mathbf{x}|\Psi) = \sum_{k=1}^{n_k} \pi_k f(\mathbf{x}; \boldsymbol{\mu}_k, \boldsymbol{\Sigma}_k) \quad (1)$$

where  $\Psi = [\boldsymbol{\pi}^T, \boldsymbol{\xi}_1^T, \dots, \boldsymbol{\xi}_{n_k}^T]^T$  is the vector that aggregates all the hyperparameters,  $\boldsymbol{\pi} = [\pi_1, \dots, \pi_{n_k-1}]^T$  is the vector of mixture proportions; vectors  $\boldsymbol{\xi}_k$  contain the hyperparameters related to the mean vector  $\boldsymbol{\mu}_k$  and the covariance matrix  $\boldsymbol{\Sigma}_k$  of the  $k^{\text{th}}$  mixture cluster; and  $f(\mathbf{x}; \boldsymbol{\mu}_k, \boldsymbol{\Sigma}_k)$  is the PDF of a multivariate Gaussian with mean  $\boldsymbol{\mu}_k$  and covariance  $\boldsymbol{\Sigma}_k$ . While the mean vector indicates the location of the center of each mixture cluster, the covariance matrix incorporates information about the variance and correlation structures of the data within each cluster.

To build the GM seismic demand model, the expectation-maximization algorithm is employed to fit the mixture model to the observed dataset. The complexity of a GM model depends on the number of clusters and the type of covariance structure adopted, which ranges from diagonal-shared to full-unshared. Therefore, the challenge in constructing the most suitable GM model resides on the selection of the number of cluster and covariance structure that fits the observed data without overfitting it. In the case of density modeling, this selection can be based on the minimum value of Bayesian information criterion (BIC) associated with the fitted models. The BIC estimates the lack of fit using the negative log-likelihood while the model complexity is penalized to avoid overfitting [14].

Advantages of this approach compared to typical MPSDMs reside on its inherent flexibility that allows a best fit to the observed data. Figure 1 illustrates an example extracted from Bandini et al. [10] for the seismic responses of bent columns and elastomeric bearings in a specific bridge. While the multivariate (MV) lognormal model fails to capture the nonlinear relationship between these two components, the GM model with  $n_k = 4$  clusters shows a better fit to the observed data at a certain IM level. Because the GM model does not necessarily rely on restrictive assumptions (e.g., lognormality and linear dependence), it allows the assessment of the impact of poor modeling and to isolate the source of bias into fragility and risk estimates.

## ESTIMATING FRAGILITY BASED ON MSA DATA

The seismic fragility of a structure reflects the conditional probability of exceeding a damage state DS given the occurrence of a seismic event with intensity  $IM = im$ , i.e.,  $\Pr(DS|IM = im)$ . A fragility function is commonly represented by the cumulative distribution function (CDF) of a lognormal distribution:

$$\Pr(DS|IM = im) = \Phi\left(\frac{\ln(im/\theta)}{\beta}\right) \quad (2)$$

where  $\Phi(\cdot)$  is the CDF of a standard normal distribution and  $\theta$  and  $\beta$  are the median and dispersion of the fragility function. An efficient strategy for fragility curve fitting using results from MSA is described by Baker [15] by maximizing the likelihood function of the fragility data obtained at multiple levels of intensity measure  $IM = y_j$ ,  $j = 1, \dots, m$ . In this case, the likelihood function is expressed as:

## 1) Multiple stripe analysis

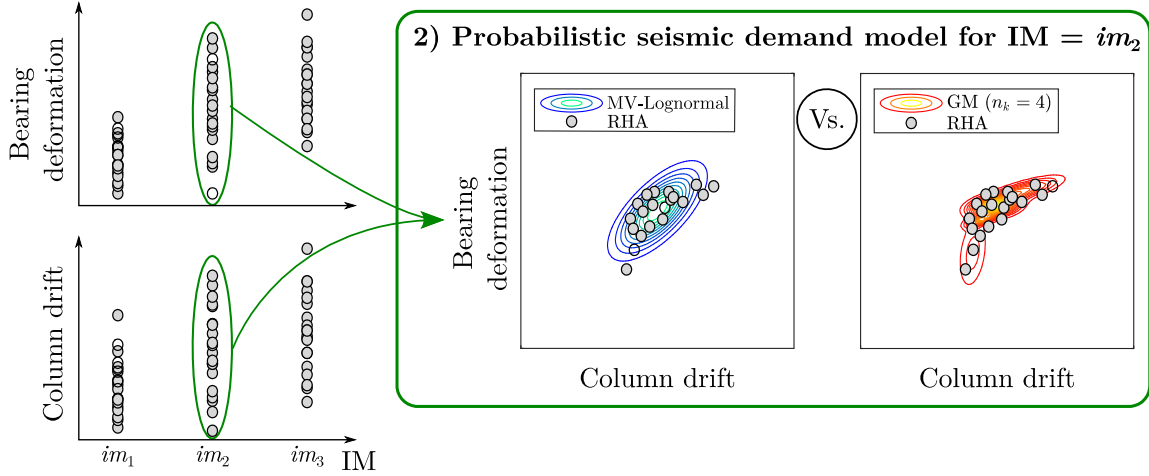


Figure 1: Comparison between PSDMs built upon a multivariate lognormal model and a Gaussian mixture model (adapted from Bandini et al. [10])

$$\text{Likelihood} = \prod_{j=1}^m \binom{n_j}{z_j} \left[ \Phi \left( \frac{\ln(im_j/\theta)}{\beta} \right) \right]^{z_j} \left[ 1 - \Phi \left( \frac{\ln(im_j/\theta)}{\beta} \right) \right]^{n_j - z_j} \quad (3)$$

where  $z_j$  is the number of cases of damage state exceedance out of  $n_j$  analyses at  $IM = y_j$ . For simplicity, the parameters of the fragility function can then be obtained using the maximum likelihood estimation on the logarithmic of the likelihood function. To assess the annual risk of exceeding a specific damage state  $DS_i$ , the mean annual frequency (MAF) of violating  $DS_i$  can be calculated by integrating the fragility function over the site hazard curve  $\lambda(IM)$  [16]:

$$\lambda(DS_i) = \int_{IM} \Pr(DS_i | IM = y) \left| \frac{d\lambda(IM)}{dIM} \right| dIM \quad (4)$$

### BOOTSTRAP SEISMIC FRAGILITY CURVES

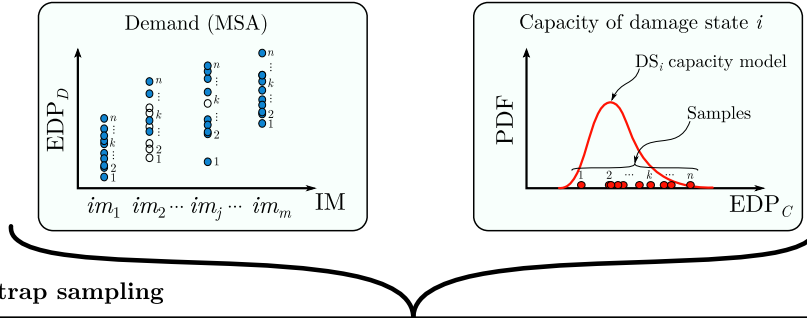
The seismic fragility of a bridge is facilitated by the assumption of series system, which means that the failure of a single component results in the system failure. A thorough approach to build system fragility functions treating uncertainty on both demand and capacity is facilitated using sampling methods, e.g., Monte Carlo sampling. In this case, the steps involved are: (1) the generation of a seismic demand dataset and fitting of joint probabilistic modeling, (2) the generation of capacity samples from probabilistic capacity models of critical components, and (3) the pairing of demand and capacity samples data to estimate the fragility. To avoid the adoption of parametric assumptions on seismic demand, a nonparametric bootstrap-based approach seems to be a suitable strategy to build fragility functions and to perform statistical inference. Bootstrapping estimates the distribution of a statistic by repeatedly resampling from the observed data with replacement [17]. Bootstrapping has already been adopted to assess the uncertainty in fragility and risk quantities within different frameworks (e.g., [16,18]).

In this study, a bootstrap procedure is proposed to incorporate the uncertainty related to the capacity of structural components (Figure 2). At first, seismic demand data  $EDP_D$  is generated using the MSA approach, while component capacity data  $EDP_C$  is sampled from a capacity model for a specific damage state  $DS_i$ . The size of the demand dataset is  $n \times m$ , where  $n$  is the number of response history analyses (RHA) in a single stripe and  $m$  is the number of intensity measure levels used in MSA (i.e., the number of stripes). In this case, the capacity dataset has  $n$  samples (i.e., the same number of RHA per stripe) (Step 1 in Figure 2). Demand and capacity data points are here labeled from 1 to  $n$  from the lowest EDP to the highest in ascending order only for simplicity. Next,  $n$  bootstrap samples are generated for both demand and capacity for each level of seismic intensity measure  $IM = im_j, j = 1, 2, \dots, m$ . These samples are then paired to compare if the demand exceeds the capacity (i.e., if  $DS_i$  exceedance occurs). Resampling and pairing are replicated for  $b = 1, 2, \dots, B$  (Step 2 in Figure 2). The bootstrap replications of the number of cases of DS exceedance  $z_{j,b}$  are then obtained, based on the series system assumption. Finally, a replication system fragility curve is fitted to the resampled fractions of ground motions causing  $DS_i$  violation at all  $m$  intensity levels (Step 3 in Figure 2). Thus, applying maximum likelihood estimation to the replication ratios  $z_{j,b}/n$ , the solution of Equation 3 takes the following form in the logarithmic transformed space:

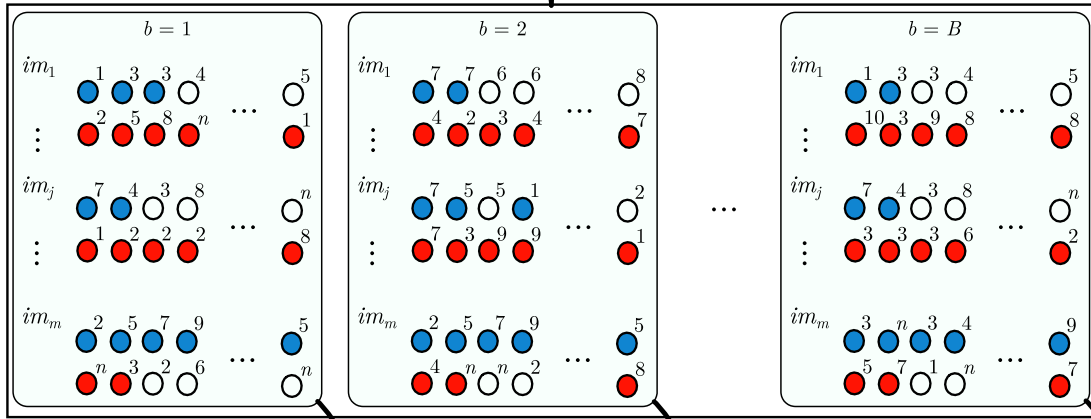
$$\{\hat{\theta}, \hat{\beta}\}_b = \arg \max_{\theta, \beta} \sum_{j=1}^m \left\{ \ln \binom{n}{z_{j,b}} + z_{j,b} \ln \Phi \left( \frac{\ln(im_j/\theta)}{\beta} \right) + (n - z_{j,b}) \ln \left[ 1 - \Phi \left( \frac{\ln(im_j/\theta)}{\beta} \right) \right] \right\} \quad (5)$$

Therefore, the nonparametric aspect of the adopted procedure to develop bootstrap fragility curves resides only on the resampled demand data, because these are the limited dataset generated from the response history analyses. The capacity models are assumed to follow lognormal distributions, and the shape of the fragility curves is assumed as the lognormal CDF given the good fit to the observed data in this study. The corresponding MAFs of damage state exceedance  $\lambda(DS)$  are then calculated according to Equation 4.

**Step 1: Generation of demand and capacity data**



**Step 2: Bootstrap sampling**



**Step 3: Fragility replications**

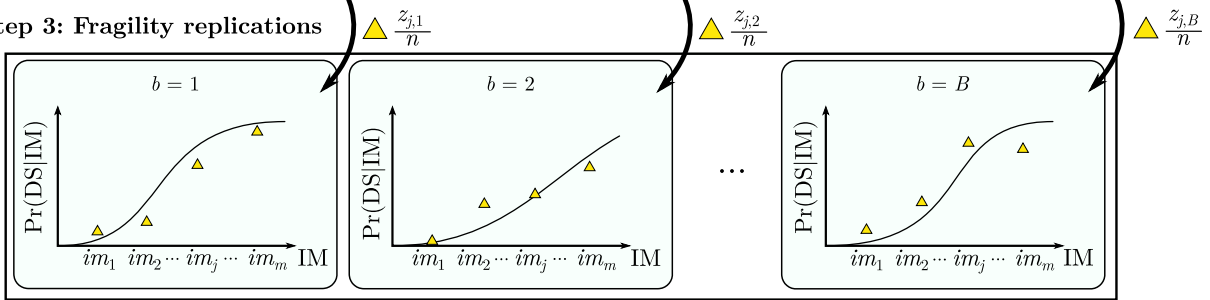


Figure 2: Methodology for the construction of bootstrap fragility curves

**CASE-STUDY BRIDGE**

This study assesses the seismic performance of a real case-study structure: the Chemin des dalles Bridge Located over highway 55 near Trois-Rivière, Quebec, Canada. Due to its regular characteristics and similarities to other provincial bridges, this structure has been extensively studied. It is a symmetric continuous concrete girder bridge with three equally spaced 35.5 m long spans and a 13.2 m wide deck. A reinforced concrete slab and six prestressed concrete AASHTO type-V girders compose the superstructure, while the substructure is formed by two three-column bents and seat-type abutments with wing walls. Girders are directly connected on the bent cap beams and rest on elastomeric bearing pads at the abutments. Pier bents are composed of circular columns (914 mm diameter) and square section cap beams, with a vertical clearance of 6.2m. A 25.4 mm gap separates the deck from the abutment wing walls and back wall.

The three-dimensional finite element model created on the Open System for Earthquake Engineering Simulation (OpenSees) [19], and it uses beam-column and zero-length elements to represent the behavior of this structural system and to capture the nonlinear behavior of critical structural components (bent columns, elastomeric bearings, and abutment wing walls). Superstructure elements, including the deck and girders, are defined as linear-elastic elements, while the substructure is constituted by the nonlinear elements and soil-structure interaction (Figure 3). Further details on the numerical model and its calibration are found elsewhere (Tavares et al. 2013).

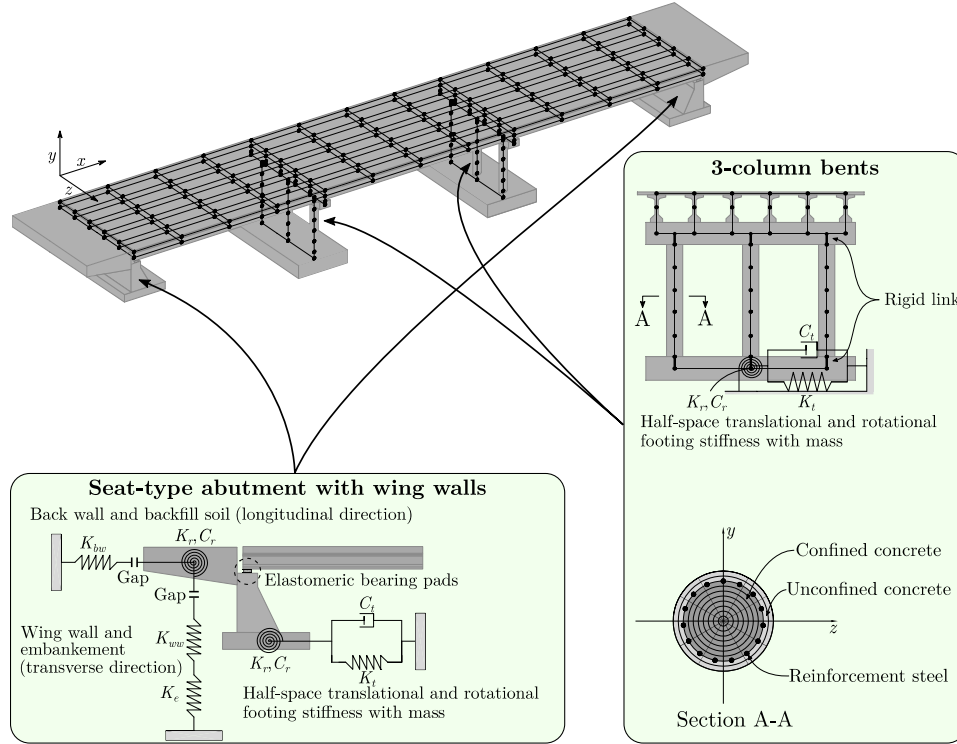


Figure 3: Numerical model of the Chemin-des-dalles Bridge built on OpenSees

The Chemin des Dalles Bridge was designed in 1975, and to reflect the seismic capacity of its reinforced concrete columns, experiment-based capacity models [20] are adopted for four damage states, i.e., minimal, repairable, extensive, and probable replacement. The capacity models for the other two critical components (abutment wing walls and elastomeric bearings) were adapted by Tavares et al. [21] for bridges in Quebec. The capacity models are assumed to follow lognormal distributions and are completely defined by median and dispersion (Table 1).

Table 1. Capacity models for the critical components of the Chemin des Dalles Bridge

Component EDP(units)	Damage state – median (dispersion)			
	Minimal	Repairable	Extensive	Probable replacement
Abutment wing walls deformation (mm)	7.0 (0.25)	15.0 (0.25)	30.0 (0.46)	60 (0.46)
Elastomeric bearings deformation(mm)	30.0 (0.25)	60.0 (0.25)	150.0 (0.46)	300.0 (0.46)
Column drift ratio (%)	0.5 (0.25)	1.4 (0.25)	2.0 (0.46)	2.2 (0.46)

For the response history analyses, ground motion records were selected using the generalized conditional intensity measure (GCIM) approach [22]. The spectral acceleration at the bridge elastic fundamental period in the transverse direction  $S_a(T_1)$  was chosen as the conditioning intensity measure at six levels: 0.2, 0.4, 0.6, 0.8, 1.0 and 1.2 g. The levels of spectral acceleration correspond to seismic events with return periods ranging from 1,400 to 44,000 years. The conditioned intensity measures were peak ground acceleration, peak ground velocity and spectral accelerations at 20 values of period ranging from 0.1 to 2.0 s to account for the effects of higher modes and period elongation due to nonlinearities. One hundred (100) ground motion records were selected at each level of conditioning  $S_a(T_1)$  from the NGA-West2 database [23]. Further details on the record selection are found in Bandini et al. [10].

## INFERENCE ON FRAGILITY AND RISK ESTIMATES

Ten thousand (10,000) bootstrap replications of the system fragility curves are performed for each of the four damage states. A subset of the bootstrap fragility curves is depicted in Figure 4 along with the fragility curves built according to three investigated MPSDM strategies: Gaussian mixture, kernel smoothing distribution, and lognormal distribution. While the GM model is the most flexible, the kernel smoothing only assumes linear dependence, and the lognormal model relies on both investigated hypotheses. For the minimal damage state, all the MPSDM-based fragility curves agree with the bootstrap replications, which in turn show a rather small variation. The 95% confidence interval (c.i.) of the median and the dispersion of the bootstrap fragility curves are inferred using percentile confidence intervals [17] (Tables 2 and 3, respectively). Effectively, the observed small variation is confirmed by the narrow confidence intervals for the minimal damage state, while the parameters of the MPSDM-based fragility curves fall within the c.i. thresholds.

These observations are not valid for the repairable and extensive damage states. Accordingly, while the fragility curves built upon the GM and kernel MPSDMs follow the general trend of the bootstrap replications, the fragility curves built upon the lognormal model deviate significantly from this trend. This graphical impression is validated by the bootstrap confidence intervals. The parameters of the lognormal model are the only that are found out of the 95% bootstrap confidence intervals, which is explained by the lack of fit of the lognormal distribution to the deformation of the abutment wing walls for intermediate levels of  $S_a(T_1)$  (see Ref. [10] for more details). Additionally, a great variation of the bootstrap fragility curves is noted for these damage states, as confirmed by the large confidence intervals of the curve parameters. This is explained by the low ratios of damage state exceedance observed for the levels of spectral acceleration adopted in this study. The fragility curves are restrained only by the lower tail, and a large variation is possible for the rest of the curve (Figures 4b and 4c). To reduce this variation, higher levels of spectral acceleration could be used [15]. For this specific case, however, this would mean using ground motions of excessively large return periods ( $> 50,000$  years) and selecting records for this order of return period that satisfactorily match the GCIM target distribution can be rather challenging [24].

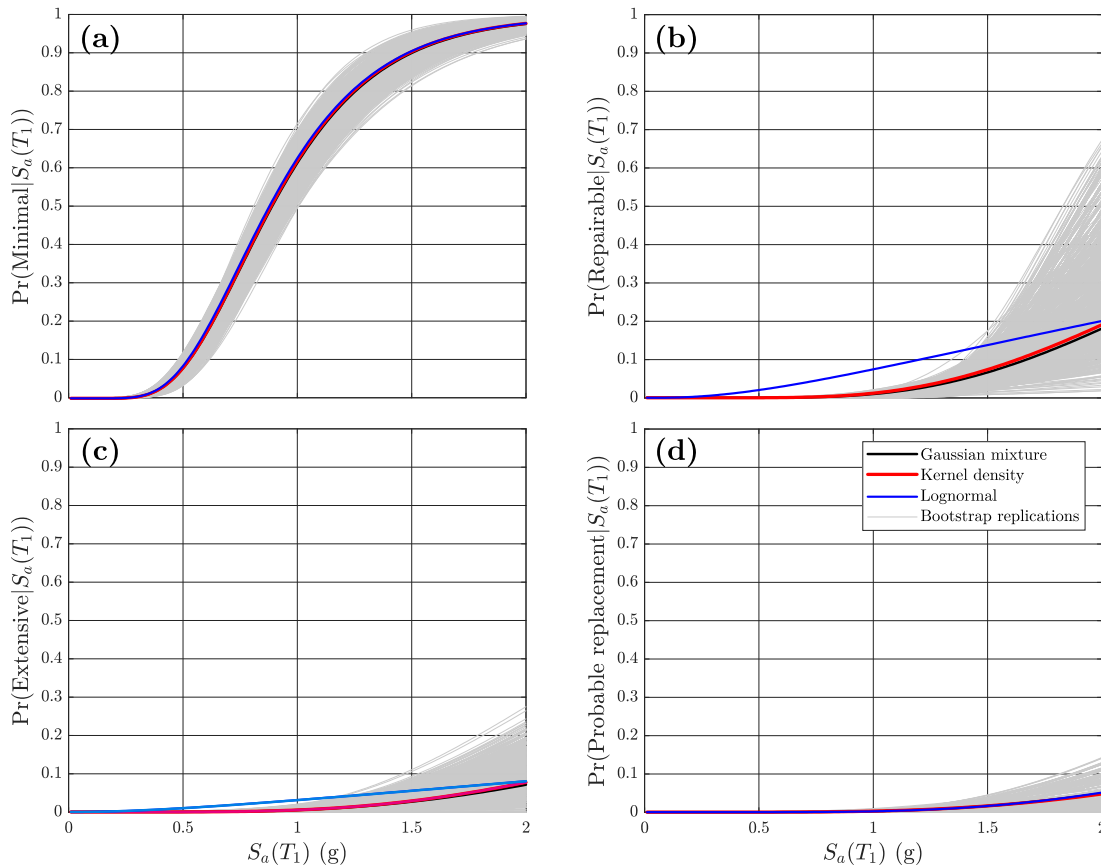


Figure 4: Comparison of fragility curves against bootstrap replications

Table 2: Comparison of the median of the fitted fragility curves to the bootstrap confidence interval (values in g)

Damage state	Bootstrap 95% c.i.	Gaussian mixture	Kernel density	Lognormal
Minimal	(0.84, 0.97)	0.89	0.88	0.87
Repairable	(1.95, 4.66)	3.12	3.09	5.13
Extensive	(3.02, 15.28)	4.88	4.62	16.46
Probable replacement	(3.63, >20)	5.22	5.62	4.98

Table 3: Comparison of the dispersion of the fitted fragility curves to the bootstrap confidence interval

Damage state	Bootstrap 95% c.i.	Gaussian mixture	Kernel density	Lognormal
Minimal	(0.39, 0.41)	0.40	0.40	0.41
Repairable	(0.24, 0.63)	0.48	0.50	1.14
Extensive	(0.47, 0.97)	0.61	0.59	1.50
Probable replacement	(0.46, 0.80)	0.58	0.62	0.56

For the probable replacement damage state, all the MPSDM-based fragility curves showed good agreement to the bootstrap fragility curves. In this case, only the columns participate on the system's fragility. Owing to the reasonably good fit of the lognormal distribution to the peak column drift ratios, the fragility curves built upon the multivariate lognormal strategy show once again a good agreement with the other curves. Although not evidenced in Figure 3, the large variation for this damage state is indicated by the wide confidence interval of the median (Table 1). Again, this large variation is justified by fitting the fragility curves with low fractions of damage state exceedance.

From the 10,000 bootstrap fragility curve replications, the corresponding mean annual frequencies of damage state exceedance are calculated for each  $DS_i$ . A standardization of the MAFs is adopted as follows to facilitate the comparison:

$$z_{\lambda(DS_i)} = \frac{\lambda(DS_i) - \bar{\lambda}(DS_i)_{boot}}{s(\lambda(DS_i)_{boot})} \quad (6)$$

where  $\bar{\lambda}(DS)_{boot}$  and  $s(\lambda(DS)_{boot})$  are, respectively, the sample mean and standard deviation of the mean annual frequency of exceeding the damage state  $DS_i$  from the bootstrap replications. It is, therefore, expected that the bootstrap standardized MAF replications are normally distributed with null mean and standard deviation equal to unity. Consequently, considering bias as the deviation of the estimated value from the expected (true) value, the bias of each PSDM strategy is here inferred as the distance of the standardized MAF from zero.

Figure 5 presents the histograms of the bootstrap replications of  $z_{\lambda(DS_i)}$  along with the standardized MAFs estimated upon each MPSDM strategy. For the minimal damage state, the MAF replications are normally distributed. This was expected given the low variation of the fragility curves, owing to the appropriate fragility ratios used to fit the curves. The good agreement of all the MPSDM-based fragility curves with the bootstrap replications are responsible for the low bias of the corresponding MAFs (Figure 5a). For the repairable and extensive damage states, the error introduced by the poor seismic demand density modeling is propagated into the MAFs based on the MV-lognormal model. In effect, while the other MPSDM strategies introduced an error that is less than one standard deviation, the bias caused by lognormality is greater than four times the standard deviation of the bootstrap replications. The histograms of the MAF replications for these damage states present negative skew, which could again be explained by fitting the fragility curves with low fractions of DS violation. For instance, in the case of the repairable damage state, fragility curves with low dispersion (the lower bound of the confidence interval is 0.24 in Table 3) are accompanied by lower medians, generating positive standardized MAF replications, which justify the negative skew (Figure 5b). The same can be inferred over the extensive damage state, whereas to a lesser extent (Figure 5c). The probable replacement damage state presents a multimodal histogram (Figure 5d), which is justified by the too low fragility fractions used to fit the curves. In this case, the large median values ( $> 20$  g) of part of the bootstrap fragility curve replications are responsible for the negative standardized MAFs. Finally, the close MAFs estimated from GM and kernel smoothing indicate that the nonlinear correlation of the demand (which is only modeled by the GM) had a low impact on the risk assessment.

## CONCLUSIONS

A nonparametric bootstrap approach is proposed to perform inference on the system fragility curves and the corresponding estimates of MAF of damage state exceedance for a case-study bridge. In this way, no assumption was made on the distribution or correlation of the seismic demand of the bridge components. This work assessed the uncertainties on the fragility analyses in a previous study by quantifying the confidence interval of the fragility curves and the potential bias caused by poor density

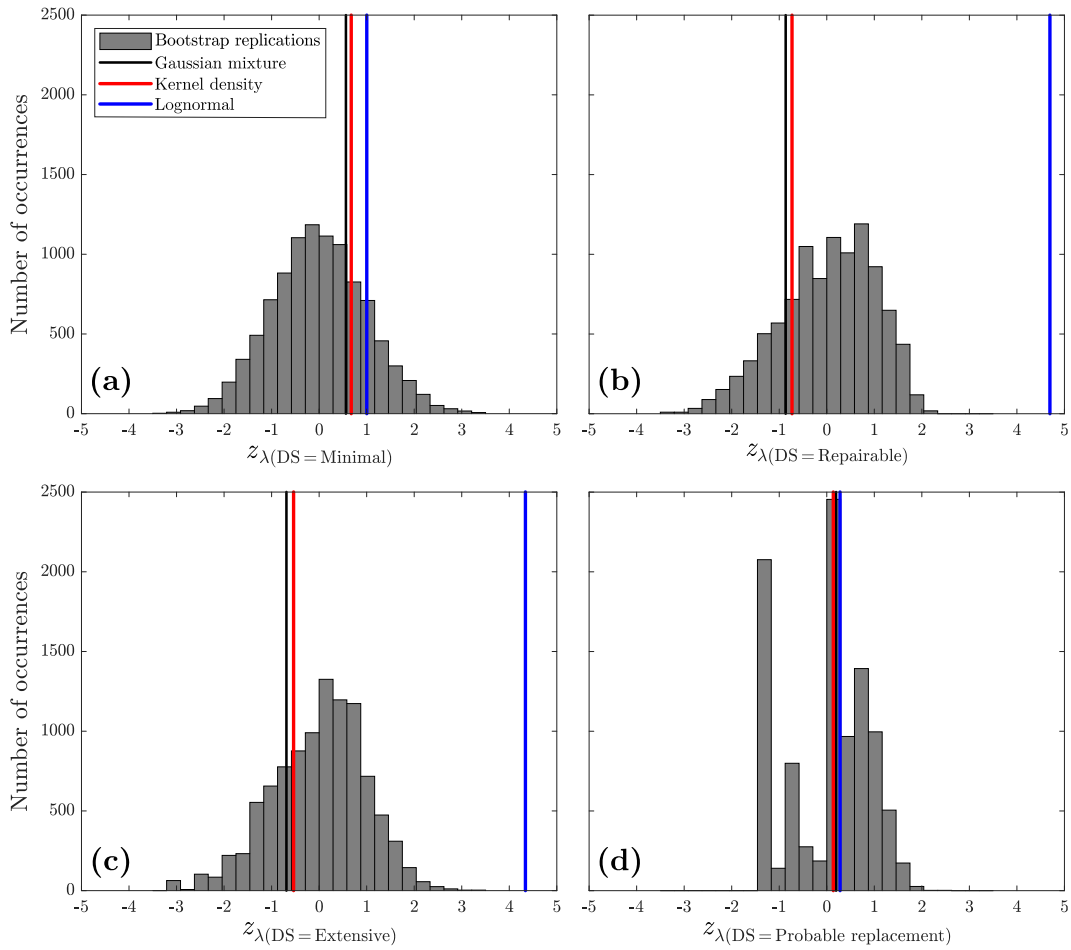


Figure 5: Comparison of standardized MAF estimates to bootstrap replications

modeling of the investigated MPSDM strategies. Ten thousand bootstrap replications were performed for each damage state, which demonstrate that only the estimated values for minimal damage state showed reasonable variability. The greater uncertainty observed for the other damage states were caused by the low fragility fractions used to fit the respective fragility curves. The large variation was carried into the estimated mean annual frequencies, whose standardized replications deviate from a standard normal distribution, especially for the probable replacement damage state. Although these results may be indicative of the need for ground motions of greater return periods, they also suggest that the Gaussian mixture model was able to capture the uncertainty of the seismic demand, propagating low error into fragility- and risk-based analyses despite the limitations relative to seismic intensity levels. The performance of the parametric GM model is comparable to the nonparametric kernel smoothing approach. This complementary study, hence, supports the initial perception that the GM model introduces lower bias than traditional MPSDM approaches, being a practical option to model the joint density of complex responses on multicomponent structures. Finally, the large variability observed for higher damage levels denotes the challenge of performing fragility and risk analyses in regions of low to moderate seismicity.

## ACKNOWLEDGMENTS

The authors gratefully acknowledge the financial support from the Natural Science and Engineering Research Council of Canada (Grant No. 37717), the Fonds de Recherche du Québec – Nature et Technologies (Grant No. 171443), and the Brazilian National Council for Scientific and Technological Development (CNPq) (Grant No. 233738/2014-2), and all the assistance provided by the Centre d'études interuniversitaire des structures sous charges extrêmes (CEISCE). Computational resources were provided by Calcul Québec and Compute Canada.

## REFERENCES

- [1] Mackie, K. R. and Stojadinovic, B. 2003. *Seismic Demands for Performance-Based Design of Bridges*. Technical Report PEER 2003/16, Pacific Earthquake Engineering Research Center, Berkeley.

- [2] Kameshwar, S., Misra, S., and Padgett, J. E. 2020. Decision tree based bridge restoration models for extreme event performance assessment of regional road networks. *Structure and Infrastructure Engineering*, **16**(3): 431-451.
- [3] Gardoni, P., Mosalam, K. M., and Der Kiureghian, A. 2003. Probabilistic seismic demand models and fragility estimates for RC bridges. *Journal of Earthquake Engineering*, **7**(S1): 79-106.
- [4] Nielson, B. G. and DesRoches, R. 2007. Seismic fragility methodology for highway bridges using a component level approach. *Earthquake Engineering & Structural Dynamics*, **36**: 823-839.
- [5] Padgett, J. E. and DesRoches, R. 2008. Methodology for the development of analytical fragility curves for retrofitted bridges. *Earthquake Engineering & Structural Dynamics*, **37**(8): 1157-1174.
- [6] Siqueira, G. H., Sanda, A. S., Paultre, P., and Padgett, J. E. 2014. Fragility curves for isolated bridges in eastern Canada using experimental results. *Engineering Structures*, **74**: 311-324.
- [7] Der Kiureghian, A. and Ditlevsen, O. 2009. Aleatory or epistemic? Does it matter? *Structural Safety*, **31**(2): 105-112.
- [8] Shome, N. 1999. Probabilistic seismic demand analysis of nonlinear structures. PhD thesis, Stanford.
- [9] Karamlou, A. and Bocchini, P. 2015. Computation of bridge seismic fragility by large-scale simulation for probabilistic resilience analysis. *Earthquake Engineering & Structural Dynamics*, **44**: 1959-1978.
- [10] Bandini, P.A.C, Padgett, J.E., Paultre, P., and Siqueira, G.H. 2022. Seismic fragility of bridges: An approach coupling multiple-stripe analysis and Gaussian mixture for multicomponent structures. *Earthquake Spectra*, **38**(1): 254-282.
- [11] Brandenburg, S. J., Zhang, J., Kashighandi, P., Huo, Y., and Zao, M. 2011. *Demand Fragility Surfaces for Bridges in Liquefied and Laterally Spreading Ground*. Technical Report PEER 2011/01, Pacific Earthquake Engineering Research Center, Berkeley.
- [12] Zhou, T., and Li, A. Q. 2019. Seismic fragility assessment of highway bridges using D-vine copulas. *Bulletin of Earthquake Engineering*, **17**(2): 927-955.
- [13] Jalayer and C. A. Cornell. Alternative non-linear demand estimation methods for probability-based seismic assessment. *Earthquake Engineering & Structural Dynamics*, **38**: 951-972, 2009.
- [14] McLachlan, G.J., and Peel, D. 2000. *Finite mixture models*. Wiley, New York, 2000.
- [15] Baker, J. W. 2015. Efficient analytical fragility function fitting using dynamic structural analysis. *Earthquake Spectra*, **31**(1): 579-599.
- [16] Eads, L., Miranda, E., Krawinkler, H., and Lignos, D. G. 2013. An efficient method for estimating the collapse risk of structures in seismic regions. *Earthquake Engineering & Structural Dynamics*, **42**: 25-41.
- [17] Efron, B. and Tibshirani, R. J. 1998. *An introduction to the bootstrap*. Chapman and Hall/CRC, Boca Raton.
- [18] Chandramohan, R., Baker, J. W., and Deierlein, G. G. 2016. Quantifying the influence of ground motion duration on structural collapse capacity using spectrally equivalent records. *Earthquake Spectra*, **32**(2): 927-950.
- [19] McKenna, F., Scott, M. H., and Fenves, G. L. 2010. Nonlinear Finite-Element Analysis Software Architecture Using Object Composition. *Journal of Computing in Civil Engineering*, **24**(1): 95-107.
- [20] Zuluaga Rubio, L. F., Le Tartesse, Y., Calixte, C., Chancy, G., Paultre, P., and Proulx, J. 2019. Cyclic behaviour of full scale reinforced concrete bridge columns. In *12th Canadian Conference on Earthquake Engineering*, Quebec City, Canada.
- [21] Tavares, D. H., Suescun, J. R., Paultre, P., and Padgett, J. E. 2013. Seismic Fragility of a Highway Bridge in Quebec. *Journal of Bridge Engineering*, **18**(11):1131-1139.
- [22] Bradley, B. A. 2010. A generalized conditional intensity measure approach and holistic ground-motion selection. *Earthquake Engineering & Structural Dynamics*, **39**: 1321-1342.
- [23] Ancheta, T. D. et al. 2014. NGA-West2 database. *Earthquake Spectra*, **30**(3): 989-1005.
- [24] Bradley, B. A. 2013. Practice-oriented estimation of the seismic demand hazard using ground motions at few intensity levels. *Earthquake Engineering & Structural Dynamics*, **42**: 2167-2185.